



The effects of astronomically forced climate change on hemipelagic carbonate sedimentation in a tectonically active setting: the Albian Mioño Formation in Castro Urdiales (Cantabria, N Spain)

Aitor Payros¹  · Naroa Martínez-Braceras¹  · Luis M. Agirrezabala¹  · Jaume Dinarès-Turell²  · Idoia Rosales³ 

Received: 2 May 2022 / Accepted: 19 September 2022 / Published online: 6 October 2022
© The Author(s) 2022

Abstract

Our understanding of the stratigraphic expression of astronomically driven climate-change cycles in the Milankovitch frequency band has improved significantly in recent decades. However, several aspects have been little studied to date, such as the nature of the climatically regulated environmental processes that ultimately control cyclic sedimentation. Similarly, relatively little is known about the expression of Milankovitch cycles in successions accumulated in tectonically active basins. In order to fill this knowledge gap, the Albian hemipelagic deposits of the Mioño Formation exposed in Castro Urdiales (Basque-Cantabrian Basin) are studied herein. These deposits were accumulated during a rifting phase with strong tectonic activity. The sedimentological, petrographic and cyclostratigraphic analysis demonstrates that, despite the synsedimentary tectonic instabilities and some diagenetic overprinting, the hemipelagic carbonate alternation was astronomically forced 110.68–110.47 Ma. Seasonality fluctuations driven by precession cycles caused periodic (20 ky) variations in the rate of carbonate productivity (abundance of pelagic calcareous plankton and micrite exported from adjacent shallow-water areas) and/or siliceous dilution (terrestrially derived siliciclastic sediment supply and siliceous particle production by sponges). These variations resulted in the formation of marly limestone beds when annual seasonality was low (i.e., boreal summer at aphelion, winter at perihelion) and the accumulation of marlstones when seasonality increased (i.e., boreal summer at perihelion, winter at aphelion). The incidence of these processes increased and decreased in line with seasonality modulation by short-eccentricity cycles of 100 ky. In conclusion, this study shows that Milankovitch cycles can be reliably recorded in hemipelagic successions accumulated in tectonically active settings if sediment gravity flows or other disturbances do not affect autochthonous sedimentation.

Keywords Albian · Basque-Cantabrian Basin · Climate · Cyclostratigraphy · Hemipelagic · Milankovitch cycles

Resumen

El conocimiento sobre la expresión estratigráfica de los ciclos de cambio climático producidos astronómicamente en la banda de frecuencia de Milankovitch ha aumentado considerablemente en las últimas décadas. Sin embargo, hay algunos aspectos de los que aún no se tiene mucha información, como la naturaleza de los procesos ambientales climáticamente regulados que, en última instancia, determinan la sedimentación cíclica. Del mismo modo, no se dispone de mucha información sobre la expresión de los ciclos de Milankovitch en sucesiones acumuladas en cuencas tectónicamente activas. Con el fin de

✉ Aitor Payros
a.payros@ehu.eus
Naroa Martínez-Braceras
naroa.martinez@ehu.eus
Luis M. Agirrezabala
l.agirrezabala@ehu.eus
Jaume Dinarès-Turell
jaume.dinares@ingv.it
Idoia Rosales
i.rosales@igme.es

¹ Department of Geology, Faculty of Science and Technology, University of the Basque Country (UPV/EHU), P.O. Box 644, 48080 Bilbao, Spain

² Istituto Nazionale di Geofisica e Vulcanologia, Via di Vigna Murata 605, 00142 Rome, Italy

³ Centro Nacional Instituto Geológico y Minero de España (IGME, CSIC), La Calera 1, Tres Cantos, 28760 Madrid, Spain

paliar estas deficiencias, en este trabajo se estudian los depósitos hemipelágicos albienses de la Formación Mioño de Castro Urdiales (Cuenca Vasco-Cantábrica), los cuales se acumularon durante una fase de rifting con fuerte actividad tectónica. El análisis sedimentológico, petrográfico y cicloestratigráfico demuestra que, a pesar de la existencia de inestabilidades tectónicas y alguna alteración diagenética, la alternancia carbonatada hemipelágica de hace 110.68–110.47 Ma estuvo regulada astronómicamente. Las fluctuaciones de estacionalidad inducidas por los ciclos de precesión causaron variaciones periódicas (20 ka) en las tasas de producción carbonatada (abundancia de plancton pelágico calcáreo y micrita exportada desde áreas someras adyacentes) y/o dilución silíceas (aporte de sedimento siliciclástico terrestre y producción de partículas silíceas por esponjas). Estas variaciones determinaron la formación de calizas margosas cuando la estacionalidad anual era baja (i.e., verano boreal en el afelio, invierno en el perihelio) y la acumulación de margas cuando aumentaba la estacionalidad (i.e., verano boreal en el perihelio, invierno en el afelio). La incidencia de estos procesos aumentaba y disminuía en consonancia con la modulación de la estacionalidad producida por los ciclos de excentricidad corta de 100 ka. En conclusión, este estudio demuestra que los ciclos de Milankovitch pueden quedar fielmente registrados en sucesiones hemipelágicas acumuladas en contextos tectónicamente activos si los flujos gravitacionales de sedimento u otras perturbaciones no afectan a la sedimentación autóctona.

Palabras Clave Albiense · Cuenca Vasco-Cantábrica · Clima · Cicloestratigrafía · Hemipelágico · Ciclos de Milankovitch

1 Introduction

The Earth's orbital trajectory around the Sun and the position of its rotational axis change regularly due to gravitational interactions with other astronomical bodies. Consequently, the seasonal and latitudinal rate of insolation (solar radiation) on the Earth's surface varies quasi-periodically, producing cyclic episodes of climate change 10^4 – 10^6 years in duration, which are generally referred to as Milankovitch cycles (e.g., De Boer & Smith, 1994; Hinnov, 2013; Laskar, 2020; Schwarzscher, 1993; Weedon, 2003). These astronomically forced climatic cycles can be registered in the stratigraphic record of climate-sensitive sedimentary environments, manifested as cyclic vertical arrangements of paleoclimatic proxies, mainly sedimentary facies and compositional parameters.

Hemipelagic deposits accumulated in relatively deep-marine environments provide some of the best examples of astronomically forced climate-change cycles, as their low-energy conditions and potentially uninterrupted sedimentation result in virtually continuous stratigraphic successions (Einsele et al., 1991; Kodama & Hinnov, 2015; Weedon, 2003). However, the number of studies investigating which climatically regulated environmental processes ultimately control the compositional variations recorded in hemipelagic deposits in response to Milankovitch cycles is still relatively low (e.g., Boulila et al., 2010; Elderbak & Leckie, 2016; Gambacorta et al., 2019; Jimenez-Berrocoso et al., 2013; Martínez-Braceras et al., 2017). In addition, the number of astronomically forced hemipelagic successions studied to date also varies depending on basinal geodynamic context. Most cyclostratigraphic studies have been carried out in tectonically stable oceanic basins or passive continental margins. However, in tectonically active settings comparatively little is known about the marine

sedimentary record of Milankovitch cycles (Cantalejo & Pickering, 2015; Fenner, 2001; Ferguson et al., 2021; Jones et al., 2019; Kodama et al., 2010; Laurin & Sageman, 2007). The most likely reason is that tectonically driven instabilities (e.g., earthquakes, tsunamis, gravitational collapses, etc.) are generally powerful, short lived and episodic, rather than periodic. Consequently, the environmental effects of these instabilities exceed those of background climate change, imprinting the sedimentary record more prominently.

Taking everything into account, this study was conceived with two objectives. Firstly, to investigate whether Milankovitch cycles can be identified in hemipelagic successions accumulated in tectonically active sedimentary basins. Secondly, to better understand which environmental processes may govern the formation of hemipelagic limestone-marlstone alternations modulated by astronomically driven climate change. In order to combine these two objectives in a single study, we focused on the Albian (Lower Cretaceous) hemipelagic successions of the Basque-Cantabrian Basin, a long-lived sedimentary basin located between mainland Europe and the Iberian microplate (Fig. 1a). The Basque-Cantabrian Basin is well known for its hemipelagic successions modulated by Milankovitch cycles, some of which are world-class references (e.g., Batenburg et al., 2012, 2014; Dinarès-Turell et al., 2003, 2014, 2018; Martínez-Braceras et al., 2022). These cyclostratigraphic studies were carried out in Upper Cretaceous and lower Paleogene successions, which were formed when the basin was going through relative tectonic quiescence. However, to date Milankovitch cycles had not been conclusively identified in older deposits. In Aptian–Albian times the Basque-Cantabrian area was a pericratonic continental to marine basin located in the Bay of Biscay proto-oceanic rift at approximately 30–35°N paleolatitude (Hay et al., 1999; Rosales, 1999). Evidence of

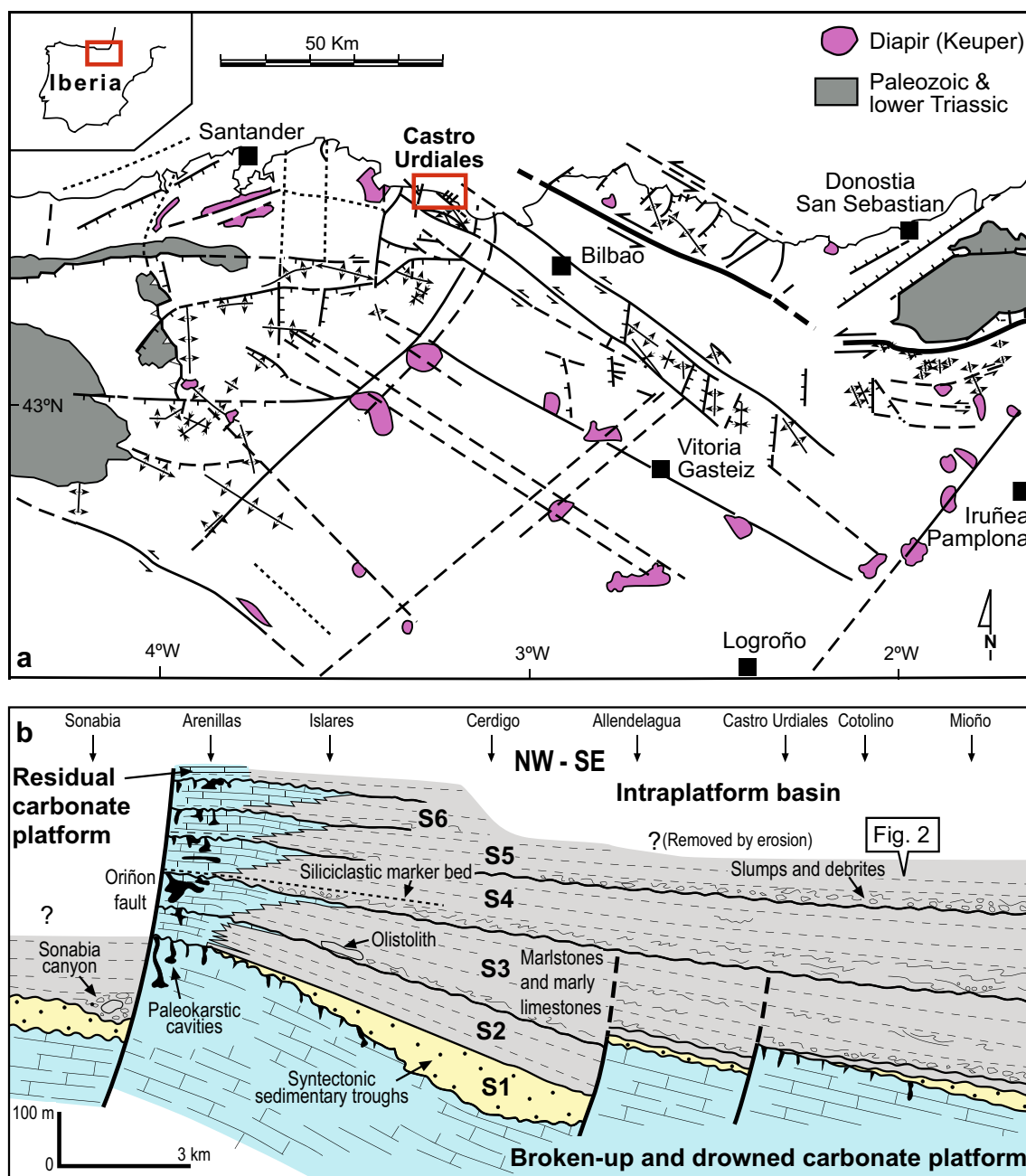


Fig. 1 **a** Map (without palinspastic restoration) of Aptian-Albian syndimentary tectonic structures of the Basque-Cantabrian area (modified from García-Mondéjar et al., 1996), with location of the studied Castro Urdiales area. **b** Stratigraphic cross-section of Albian deposits in the Castro Urdiales area highlighted in **a** (modified from Rosales et al., 1994, and Rosales, 1999), with location of the Cotolino-Mioño section studied herein. Albian tectonic activity caused the break-up of a former carbonate platform (blue), creating fault-bounded blocks tilted south-eastwards. The crest of one of

these blocks formed a paleohigh that allowed the nucleation and growth of the residual Arenillas-Islares carbonate platform, which became subaerially exposed and karstified during pulses of tectonic uplift. The residual platform was surrounded by intraplateform basinal deposits of the Pobeña Formation (sandy calcarenites in yellow) and the Mioño Formation (mainly hemipelagic limestone-marlstone alternations in grey). Resedimented deposits accumulated during periods of block tilting. S1 to S6 refer to depositional sequences defined by Rosales et al. (1994) and Rosales (1999)

strong syndimentary faulting, volcanism and hydrothermal activity is widespread and abundant here (e.g., Agirrezabala, 2015; Bodego & Agirrezabala, 2013; Fernandez-Mendiola & Garcia-Mondejar, 1995; García-Mondéjar et al., 1996;

Lopez-Horgue et al., 2010). In this environmentally unstable context, hemipelagic limestone-marlstone alternations accumulated in some deep-water sites, such as the Albian Cotolino-Mioño section in Castro Urdiales (autonomous

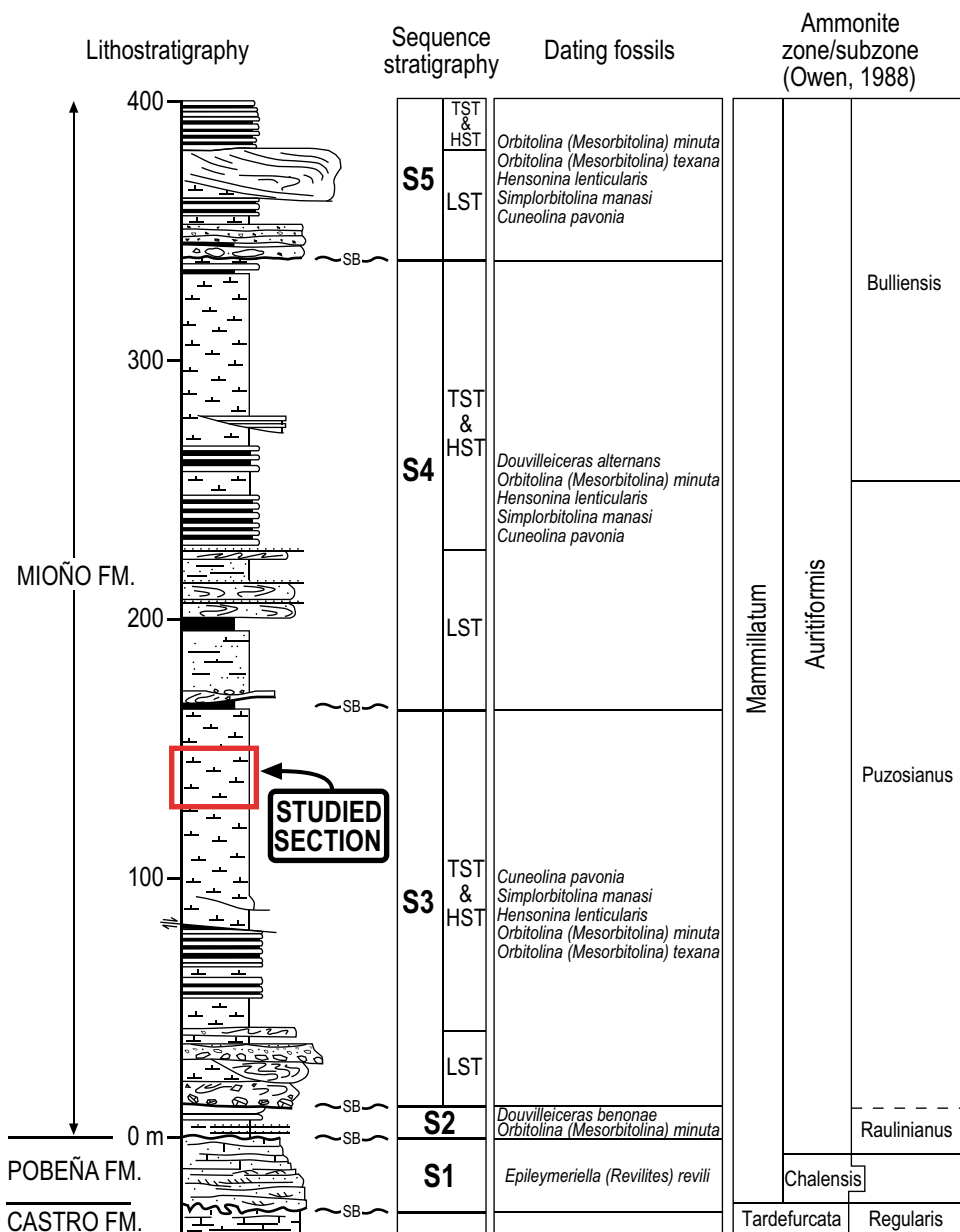
community of Cantabria, northern Spain; Fig. 1b). Both diagenetic and astronomical factors were suggested as possible drivers of this hemipelagic alternation, but neither could be definitely demonstrated (Rosales, 1995, 1999). Consequently, the Castro Urdiales area was revisited with the aim of further analysing its hemipelagic sedimentary alternations.

2 Geological setting

In Aptian–Albian times, a warm and humid subtropical climate, combined with active extensional and/or transtensional faulting (Agirrezabala, 2015; Bodego &

Agirrezabala, 2013; García-Mondéjar et al., 1996; Miró et al., 2021; Tavani & Muñoz, 2012), allowed the formation of coralgall and rudist carbonate platforms on uplifted blocks of the Basque-Cantabrian Basin. Simultaneously, deeper water hemipelagic and resedimented deposits accumulated in intervening troughs (e.g., Agirrezabala & García-Mondéjar, 1992; García-Mondéjar et al., 1996). One such carbonate platform occurred in the Castro Urdiales area (Rosales, 1995, 1999; Rosales et al., 1994, 1995). Intensified faulting in Albian times caused further fragmentation of the Castro Urdiales platform and, consequently, shallow-water carbonate sedimentation was restricted to crest areas on top of small, tilted footwalls (Fig. 1). The Arenillas-Islares residual carbonate platform, which was 2 km wide

Fig. 2 Lithological log, biostratigraphy and sequence stratigraphy of the Cotoño-Mioño section (based on data from Rosales, 1995), with indication of the interval studied herein. Location in Fig. 1b



and 300 m thick, was bounded by the Oriñon fault and the Sonabia canyon on its abrupt western margin (Rosales, 1995). The tilted eastern margin showed a low-angle homoclinal ramp-like profile on which rudist and coralgall limestones and grainstones graded into planar microsolenid coral wackestones over several hundreds of meters, and then into lithistid and hexactinellid sponge mud mounds below approximately 40 m water depth (Rosales et al., 1995). The extensive growth and exceptional preservation of siliceous sponge communities was linked to the proximity of the depositional site to mineralized hydrothermal vents along the faulted axis of the rift basin. These shallow-water deposits systematically prograded eastwards, but sedimentation was temporarily interrupted during recurrent episodes of fault reactivation, block tilting and relative sea-level drop. The consequent subaerial exposure episodes resulted in the creation of extensive karstification surfaces in the Arenillas-Islares limestones, which allowed the definition of six depositional sequences (S1 to S6 in Fig. 1b; Rosales et al., 1994; Rosales, 1995, 1999).

Further downslope, equivalent deposits mainly consisted of alternating, centimetre-to-decimetres-thick marlstone and marly limestone beds rich in planktonic foraminifera and sponge spicules (Mioño Formation as defined by Rosales, 1995; Fig. 1b). Macrofauna includes echinoids, brachiopods and scattered ammonites, and trace fossils are abundant (mainly *Chondrites*, *Zoophycos* and spreiten burrows of irregular echinoids) (Rosales, 1995, 1999). Interspersed resedimented deposits occur throughout the Mioño Formation, but olistoliths, debrites, slumps and turbidites containing shallow-water clasts, some of which show subaerial exposure features, occur at specific stratigraphic levels (Fig. 1b). These resedimentation intervals gradually thin out towards the Arenillas-Islares shallow-water platform and physically correlate with the subaerial exposure surfaces (Rosales, 1999; Rosales et al., 1994). Accordingly, the resedimentation wedges of the Mioño Formation were considered lowstand systems tracts formed during pulses of tectonic tilting, whereas the intervals dominated by hemipelagic alternations were interpreted as undifferentiated transgressive and highstand systems tracts.

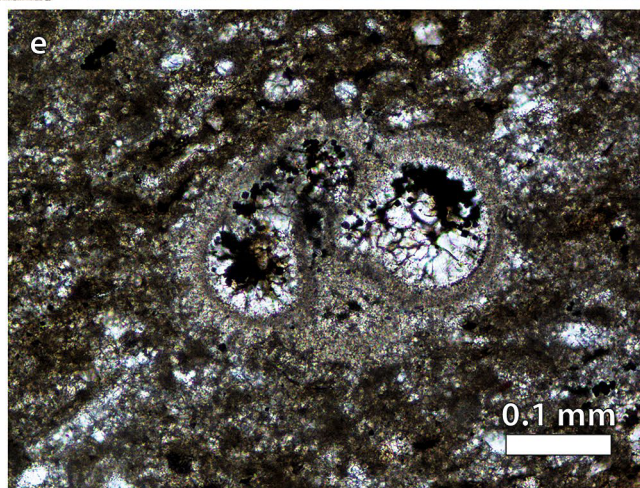
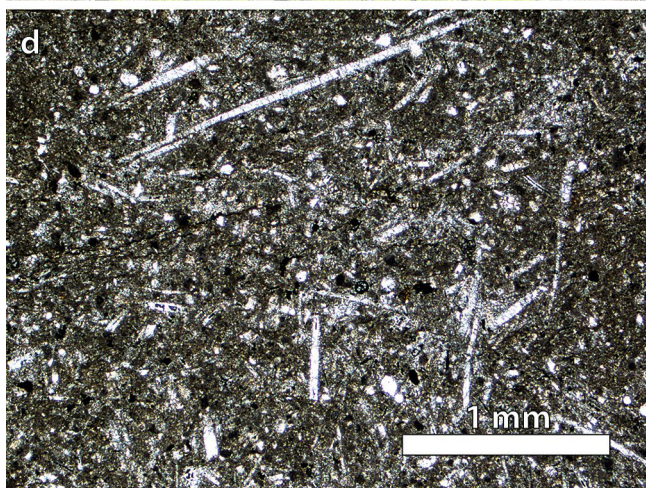
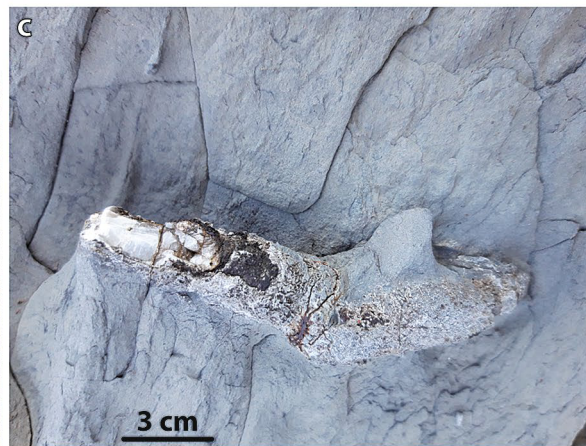
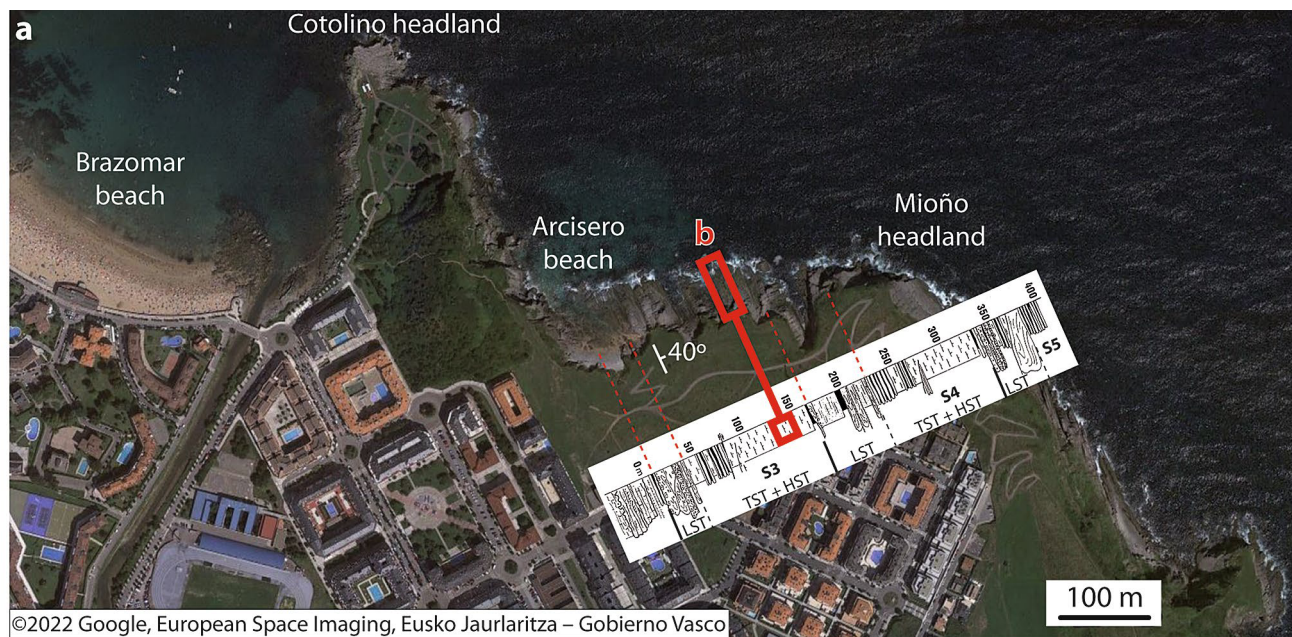
Available biostratigraphic information (Rosales, 1995) shows that the lower part of Sequence S1 contains *Epileymeriella (Revilites) revile* Jacob, which characterizes the early Albian Tardefurcata Zone, Regularis Subzone (Fig. 2). Sequence S2 contains *Douvilleiceras benonae* Besaire and *Orbitolina (Mesorbitolina) minuta* Douglass. Sequence S3 contains *Cuneolina pavonia* D'Orbigny, *Simplorbitolina manasi* Ciry & Rat, *Hensonina lenticularis* Henson, *Orbitolina (Mesorbitolina) minuta* Douglass and *Orbitolina (Mesorbitolina) texana* Roemer. Sequence 4 contains *Douvilleiceras alternans* Casey at the lower part, *Orbitolina (Mesorbitolina) minuta* Douglass, *Hensonina*

lenticularis Henson, *Simplorbitolina manasi* Ciry & Rat and *Cuneolina pavonia* D'Orbigny. These assemblages can be attributed to the early Albian Auritiformis Zone of the Mammillatum Superzone. In particular, the identification of *Douvilleiceras benonae* Besaire in Sequence S2 suggests the earliest Raulinianus Subzone, whereas the occurrence of *Douvilleiceras alternans* Casey in Sequence S4 suggests the younger Puzosianus Subzone, which most likely also includes Sequence S3 (Fig. 2). Sequence S5 yielded *Simplorbitolina manasi* Ciry & Rat, *Cuneolina pavonia* D'Orbigny, *Orbitolina (Mesorbitolina) texana* Roemer, *Orbitolina (Mesorbitolina) minuta* Douglass and *Hensonina lenticularis* Henson, whereas the overlying Sequence S6 contains *Hensonina lenticularis* Henson, *Orbitolina (Mesorbitolina) texana* Roemer, *Neorbitolinopsis conulus* Douvillé and *Dictyoconus (carinoconus) casterasi* Bilotte & Alii. Accordingly, Sequences S5 and S6 were assigned to the early-middle and late Albian, respectively.

The deposits studied herein are part of the Cotolino-Mioño section, which is exposed at the cliff between the Cotolino and the Mioño headlands in Castro Urdiales (Rosales, 1995, 1999; Rosales et al., 1994). The section is located 13 km to the east of the Arenillas-Islares carbonate platform and displays a 400 m-thick succession of the Mioño Formation (Figs. 1b, 2). Based on the 1° dip estimated for the ramp profile (Rosales et al., 1995), an original water depth of about 225 m can be calculated for the area, which largely agrees with previous estimates of 250 m for equivalent successions (García-Mondéjar, 1990; Rosales, 1995, 1999). The Mioño Formation includes three main resedimentation intervals in the Cotolino-Mioño section, each several tens of metres thick, attributed to the lowstand systems tracts of depositional sequences S3, S4 and S5 (Figs. 1b, 2). The deposits studied herein are located at approximately the 140–150 m interval of the Cotolino-Mioño section and form part of the undifferentiated transgressive and highstand systems tracts of depositional sequence S3 (Figs. 1b, 2).

3 Material and methods

With the aim of investigating a possible astronomical forcing on the origin of the outer ramp hemipelagic alternation of the Albian Mioño Formation, an 8-m-thick stratigraphic interval was analyzed around the 140 m level of the Cotolino-Mioño section (Fig. 3), which is exposed approximately 150 m to the east of the Arcisero beach in Castro Urdiales (43° 22' 25" N 3° 12' 09" W; UTM 30N X483.584 Y4.802.338). The interval was selected based on quality of exposure, definition of the alternation of recessive marlstones and weather-resistant marly limestones, accessibility, and ease of sampling. Given the decimetric thickness of the alternating marlstone



and marly limestone beds, it was considered that 8 m of stratigraphic thickness should include an adequate number of beds to test whether regular amplitude and frequency variations of compositional parameters occurred in

response to modulation by Milankovitch cycles of different periodicities (Kodama & Hinnov, 2015; Weedon, 2003). In this regard, the carbonate/clay ratio of hemipelagic sedimentary successions is commonly considered a proxy

Fig. 3 **a** Location of the studied deposits on a Google Earth view of Castro Urdiales (©2022 Google, European Space Imaging, Eusko Jaurlaritza–Gobierno Vasco; north is to the top) and on the stratigraphic succession of the Cotoño-Mioño section. **b** General view of the studied outcrop (location in **a**) with indication of the 8-m-thick hemipelagic limestone-marlstone alternation sampled for this work. Limestone beds are numbered in ascending stratigraphic order (stratigraphic top to the left). **c** Example of a cylindrical structure coated with iron oxides and with a central axis of sparry calcite. These structures, being perpendicular to bedding (stratigraphic top to the left), were most likely formed by early fluid escape from the sediments. **d, e** Optical microscope views (parallel nicols) of the studied hemipelagic deposits showing a wackestone with randomly oriented monoaxone sponge spicules, many of which are calcified (**d**), and a wackestone with a foraminifera test whose chambers are filled with sparry calcite and pyrite (**e**)

for carbonate productivity, dissolution, or siliciclastic dilution, all of which can be related to varying seawater physicochemical conditions modulated by astronomically driven climate change (Einsele & Ricken, 1991; Kodama & Hinnov, 2015; Martínez-Braceras et al., 2017).

For the compositional analysis of the studied deposits, a lithostratigraphic log was measured, in which 24 alternating marlstone and marly limestone beds with gradational boundaries were defined visually (Fig. 3b). Ten hand samples from representative marlstone and marly limestone beds were subsequently collected to prepare thin sections for petrographic analysis. In addition, another 68 samples of 25–50 g (two or three samples per bed, depending on individual bed thickness) were collected for bulk low-field magnetic susceptibility measurements, a non-destructive analytical technique carried out using a Kappabridge MFK-1 (Agico) instrument housed at the University of the Basque Country. Weight-normalized results were expressed as mass susceptibility (m^3/kg). Magnetic susceptibility of hemipelagic deposits is commonly determined by paramagnetic phases (mostly detrital clays) and generally anticorrelates with carbonate content, thus allowing spectral analysis of alternating successions for cyclostratigraphy (Kodama & Hinnov, 2015). However, the magnetic susceptibility records obtained from the studied succession showed no correlation with the hemipelagic alternation (see results below), making them unreliable for cyclostratigraphic analysis. To overcome this issue, a calcimetric analysis was carried out using the 68 hand samples of the magnetic susceptibility analysis plus another 10 samples. To this end, each hand sample was washed and dried in the laboratory, and powder samples were extracted using a W&H Perfect 300 microdrill, avoiding weathered areas, macroscopic skeletal components, burrows and veins. One gram of powder of each sample was weighed on a high-precision (three-decimal) Sartorius TE153S electronic balance, and their carbonate percentage was measured using a FOGL digital calcimeter (BD inventions), which determines the

pressure of the CO_2 gas produced from samples attacked with HCl 6 N and converts the result to $\%\text{CaCO}_3$ with an accuracy of 0.5%.

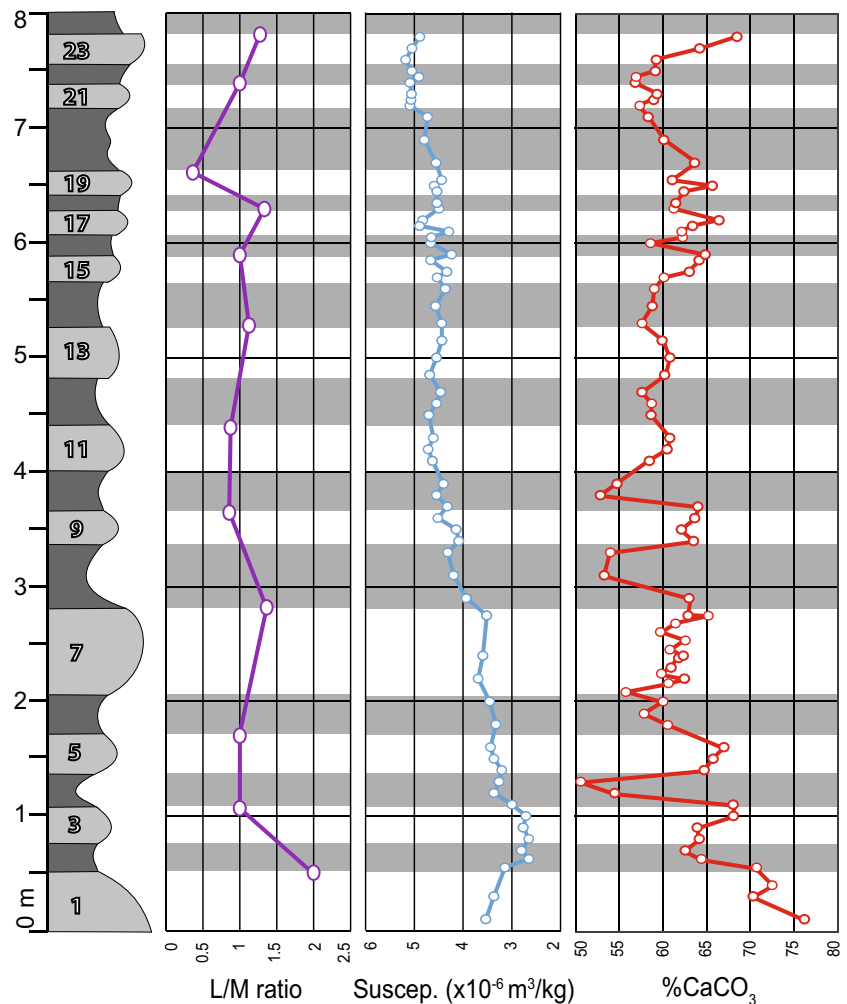
Given that the CaCO_3 measurements correlate well with the lithostratigraphic succession (see results below), the calcimeter record was analyzed for cyclostratigraphy using Acycle software (Li et al., 2019; available at <https://acycle.org/>). As samples were not evenly distributed along the succession, the $\%\text{CaCO}_3$ record was linearly interpolated first (average spacing of 10 cm) and the linear regression trend was subsequently subtracted. A power spectrum analysis of the detrended data series was carried out following the 2π -Multi Taper Method (MTM) with three tapers, and confidence levels were calculated using robust red-noise modelling (Mann & Lees, 1996; Meyers, 2012; Thomson, 1982). In addition, an Evolutive Harmonic Analysis (EHA; Thomson, 1982), which follows MatLab's Fast Fourier transform method, was carried out in order to identify distinctive frequency and amplitude modulations throughout the succession. As the succession is relatively short, the EHA was focused on the analysis of short periodicities. Therefore, a 2 m sliding window with steps of 0.1 m was used (see below). For comparison purposes, an additional EHA of the orbital solutions published for the 400–800 ka interval was carried out using an 80 ky sliding window and 1 ky steps. To this end, the astronomical solutions by Laskar et al., (2004, 2011) were used rather than the more recent solution by Zeebe and Lourens (2019), as this does not include precession cycles; the analysis was restricted to the 400–800 ka interval on the basis of its well-defined eccentricity, obliquity and precession cycles. Subsequently, Gaussian bandpass filtering of the studied $\%\text{CaCO}_3$ data series was carried out in order to isolate the signal of the most significant frequencies.

4 Results

4.1 Sedimentology and stratigraphy

The 8-m-thick stratigraphic succession contains 24 alternating recessive marlstone beds and weather-resistant marly limestone beds with gradational bounding surfaces (Figs. 3b, 4). Macroscopic sedimentary features are scarce, but centimetre-sized burrows (*Zoophycos*, *Chondrites*) are present on some bedding surfaces. In addition, cylindrical structures perpendicular to bedding, approximately 2–3 cm in diameter and up to 20 cm in length, also occur in some beds (Fig. 3c). These structures, commonly coated with iron oxides, have a central axis composed of large, radial sparite crystals that grew inwards from the external wall, although structures with semi-hollow cavities also occur.

Fig. 4 Stratigraphic log of the 8-m-thick sedimentary succession studied in the Cotoño-Mioño section, showing bed lithology (light grey: marly limestone beds, numbered as in Fig. 3b; dark grey: marlstone beds), limestone/marlstone (L/M) thickness ratio, bulk low-field mass magnetic susceptibility (expressed as m^3/kg), and $\% \text{CaCO}_3$ content. The limestone-marlstone alternation is well represented by the $\% \text{CaCO}_3$ record but not by magnetic susceptibility, showing that this characteristic was not determined by the abundance of detrital clay minerals



The petrographic analysis showed that the deposits mainly correspond to burrowed wackestones rich in randomly oriented monoaxone sponge spicules, many of which calcified (Fig. 3d). Additional components, which occur in variable proportions, include silt-sized quartz grains, planktonic and benthonic foraminifera tests, commonly with pyrite-filled chambers, and echinoderm, mollusc and brachiopod fragments. The main difference between marlstones and marly limestones is related to the abundance of clayey/silty matrix, which is generally higher in marlstones.

Beds range in thickness between 15 cm (marlstone bed 18) and 75 cm (marly limestone bed 7), averaging out at 34 cm (Online Resource 1). There is no significant difference in the thickness range of marlstone and marly limestone beds, meaning that thicker and thinner beds are not lithology dependent. The marly limestone-marlstone thickness ratio of successive beds varies between 0.4 and 2, showing no significant trends along the succession (Fig. 4).

4.2 Magnetic susceptibility

Weight-normalized magnetic susceptibility values range from $2.22 \times 10^{-6} \text{ m}^3/\text{kg}$ (marlstone bed 2) to $5.28 \times 10^{-6} \text{ m}^3/\text{kg}$ (marly limestone bed 23), averaging out at $4.15 \times 10^{-6} \text{ m}^3/\text{kg}$ (Fig. 4; Online Resource 2). Marly limestone samples yielded values ranging from 2.43×10^{-6} to $5.28 \times 10^{-6} \text{ m}^3/\text{kg}$ (average $4.1 \times 10^{-6} \text{ m}^3/\text{kg}$), whereas values from marlstone samples varied between 2.22 and $5.09 \times 10^{-6} \text{ m}^3/\text{kg}$ (average $4.12 \times 10^{-6} \text{ m}^3/\text{kg}$).

The distribution of magnetic susceptibility values along the succession shows a decreasing trend at the base (first metre), followed by a general increase up to the top of the section (Fig. 4). However, there is no correlation between the magnetic susceptibility record and the bed lithology defined in the field. For example, the lowest magnetic susceptibility value ($2.22 \times 10^{-6} \text{ m}^3/\text{kg}$) was obtained in one of the marlstone samples which should have yielded the highest values if magnetic susceptibility had truly been related to paramagnetic phases included in detrital clay minerals. Conversely, the highest value recorded in the studied

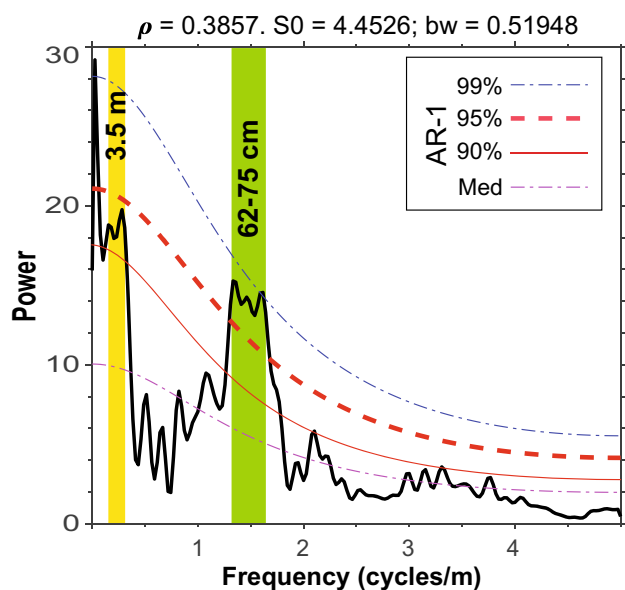


Fig. 5 2π -MTM power spectrum (black line) of the detrended $\%CaCO_3$ record derived from the studied succession, plotted in the frequency domain, showing median, 90%, 95% and 99% confidence levels for a red noise test (a fitted AR1 process). The green and yellow areas include significant peaks (with their period values above) that exceed 95% and 90% confidence levels, respectively. The ca. 69 cm peak corresponds to the average thickness of the hemipelagic limestone-marlstone couplets and is interpreted as precession driven cyclicity of ca. 20 ky, whereas the 3.5 m peak is attributed to short-eccentricity cycles of 100 ky

succession ($5.28 \times 10^{-6} \text{ m}^3/\text{kg}$) was obtained from one of the marly limestone samples expected to provide the lowest values. Taking everything into account, it was concluded that the magnetic susceptibility of the studied samples is not determined by detrital clay minerals, but rather by other magnetic phases (most likely diagenetic sulphides and iron oxides identified in the sedimentological and petrographic studies), rendering the magnetic susceptibility record invalid for the time series analysis.

4.3 $CaCO_3$ content

The carbonate content of the studied samples varied between 50.67% (marlstone bed 3) and 76.27% (marly limestone bed 1), averaging out at 61.6% (Fig. 4; Online Resource 3). Marly limestone samples yielded values ranging from 55.93 to 76.27% (average 62.99%), whereas values from marlstone samples varied between 50.67 and 70.76% (average 59.6%). The overlap in carbonate content of recessive marlstone beds and weather-resistant marly limestone beds shows that each lithology cannot be defined by a precise $\%CaCO_3$ value.

Interestingly, however, the carbonate content record fluctuates in line with the hemipelagic alternation defined visually in the field (Fig. 4). Thus, each marlstone bed has

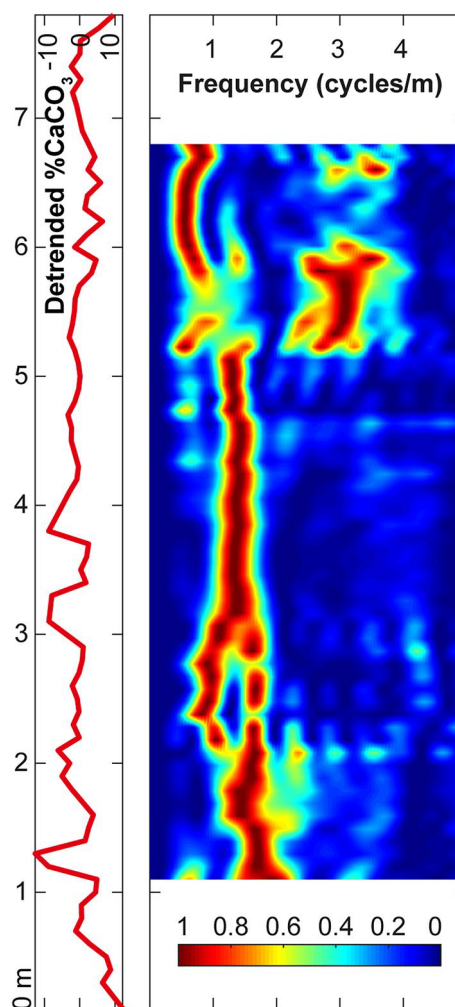


Fig. 6 Evolutive harmonic analysis of the detrended $\%CaCO_3$ record of the studied succession (in red in the left-hand side graph) using a sliding window of 2 m with steps of 0.1 m and no zero-padding. The evolutionary spectrum shows a dominant spectral band centred at a period of approximately 0.7 m, which corresponds to the average thickness of the hemipelagic limestone-marlstone couplets that represent precession cycles. This frequency band forks into two separate bands, one with higher power and the other with lower power, at the 2–3 m and 5.5–6.5 m stratigraphic intervals

lower $\%CaCO_3$ values than the underlying and overlying marly limestone beds, whereas each marly limestone bed has higher values than the underlying and overlying marlstone beds. This means that the $\%CaCO_3$ record reliably reflects the compositional variations of the studied succession. Most of the exceptions (outliers) corresponded to samples collected at the gradational boundaries between beds, and allowed more accurate redefinition of the stratigraphic position of such boundaries. In addition, results from marly limestone bed 7 showed subtle internal fluctuations, suggesting that this exceptionally thick bed might actually be a composite bed containing several amalgamated layers of

alternating marlstones and marly limestones, among which the contrast in %CaCO₃ is lower.

4.4 Time series analysis

As the %CaCO₃ record correlates well with the lithostratigraphic succession, it was used for spectral analysis at the depth domain. The 2 π -MTM power spectrum of the linearly interpolated (resolution: 0.1 m) and linearly detrended %CaCO₃ data series shows a prominent double peak between 0.75 and 0.62 m period bands (average of 0.69 m), the former exceeding 95% confidence level and the latter reaching 99% (Fig. 5). Another less prominent peak, but still above 90% confidence level and almost reaching 95%, occurs at the 3.5 m period band.

Based on the most reliable periods identified in the 2 π -MTM power spectrum, an EHA was carried out. In order to focus on the lower period cyclicity, the EHA was carried out using a 2 m sliding window and 0.1 m steps (Fig. 6). Zero padding was not applied in order to avoid potential artefacts. The evolutionary spectral analysis shows a dominant spectral band centred at approximately 0.7 m period. However, this main period band shows bifurcations at the 2–3 m and 5.5–6.5 m stratigraphic intervals, in which the main band forks into two period bands, one with higher power and the other with lower power.

5 Discussion

5.1 Astronomical forcing

The sedimentary and petrographic characteristics of the studied deposits suggest that they accumulated in well-oxygenated, low-energy, aphotic marine conditions, an interpretation in line with hemipelagic sedimentation occurring at an estimated water depth of 225–250 m. Regular hemipelagic lithological alternations can be formed either as a response to periodic fluctuations in depositional conditions driven by astronomically forced climate-change cycles (e.g., Batenburg et al., 2012, 2014; Boulila et al., 2010; Dinarès-Turell et al., 2003, 2014) or as a result of diagenetic dissolution/cementation processes during burial (e.g., Mount & Ward, 1986; Reuning et al., 2005, 2006; Westphal et al., 2004, 2010).

Diagenetic overprinting is evident in the studied deposits, as shown by the occurrence of pyrite and iron oxides, which affected the magnetic susceptibility record. These mineral phases are mainly restricted to the chambers of foraminifera tests (Fig. 3e), suggesting that their formation was related to redox reactions during organic matter decay. It can therefore be assumed that such reactions did not affect

the composition of the surrounding carbonate matrix. The effects of carbonate diagenesis are recorded by the sparite-filled cylindrical structures perpendicular to bedding, which were most likely formed by fluid escape, the abundance of calcified sponge spicules, and the foraminifera tests that are usually recrystallized with calcite overgrowths and the micritic matrix in their chambers locally transformed into microspar (Fig. 3). Post-depositional processes in alternating limestone-marlstone successions generally result in differential diagenesis, as aragonitic components are selectively dissolved from marlstone layers, leading to increased compaction, and calcite cement precipitates in adjacent limestone layers (Westphal et al., 2010). In the studied deposits, both macroscopic and microscopic dissolution features are scarce. In addition, monoaxone sponge spicules are randomly oriented in both marlstone and limestone beds, suggesting that the succession has not been affected by differential compaction. Similarly, there is no difference in the concentration of calcitic foraminifera from marlstone and limestone beds. Their preservation is also similar in both lithologies, fragile tests squashed due to (differential) compaction being rare. Furthermore, the studied beds are laterally continuous at outcrop scale and do not show nodular or lenticular features, which are usually common in successions affected by strong diagenetic dissolution/cementation processes (Hallam, 1986; Preto et al., 2005; Westphal et al., 2010). As evidence is mainly restricted to sponge spicules and foraminifera tests, carbonate recrystallization having a widespread strong impact on the studied succession can be discounted. Rather, carbonate redistribution was most likely related to organic matter decay and localized intrabed fluid flow during early diagenesis. Accordingly, several studies have suggested that hemipelagic limestones and marlstones that became indurated during early diagenesis may represent closed systems that retain primary signals, especially where the calcite/organic matter ratio is high (Marshall, 1992; Schmitz et al., 2001). Consequently, the carbonate content found in each bed can be considered to generally reflect the original composition of the sediment. In conclusion, the sedimentological and petrographic evidence suggests that the studied hemipelagic alternation was not formed by diagenetic processes.

Extensional faults can also play a significant role in cycle formation, as differential subsidence in tilted blocks can control accommodation space and thus affect shallow-water carbonate production and offshore export. Based on actual data from Quaternary extensional settings, forward tectono-stratigraphic modelling and numerical simulations of peritidal carbonate parasequences showed that the activity of extensional faults can result in the formation of high-frequency, metre-scale cycles (De Benedictis et al., 2007). In particular, cycles formed in hangingwall sites were

shown to be either asymmetric (shallowing-upward) or symmetric (deepening then shallowing upward), and of the same thickness, frequency and bathymetric trends as cycles commonly interpreted to be due to orbitally driven eustatic sea-level changes or autocyclic processes. However, such a tectonic triggering can be excluded for the cycles identified in this study, as the vertical arrangement of facies shows no distinctive bathymetric trend.

The 2π -MTM power spectrum carried out with the %CaCO₃ record of the studied hemipelagic alternation highlights the occurrence of a significant period band centred at approximately 70 cm, which coincides with the average thickness of the observed marly limestone-marlstone couplets (Fig. 5). In addition, the 2π -MTM power spectrum shows the occurrence of another significant cyclicity with a period of approximately 3.5 m. The confidence level of this larger-scale cyclicity is lower than that of the lithological alternation, but this can be attributed to the studied succession being relatively short. The 1:5 ratio between the two periodicities identified by spectral analysis has no significance in relation to extensional tectonics, but is typical of astronomical forcing on sedimentation by short-eccentricity cycles (average duration of 100 ky) and precession cycles (average duration of 20 ky). This shows that the astronomically driven climatic signal was recorded in the Mioño Formation when sediment gravity flows or other disturbances did not affect autochthonous sedimentation. The absence of any clear spectral evidence of obliquity cycles was to be expected, as these are known to mainly affect high latitudes or cold regions (De Boer & Smith, 1994; Hinnov, 2013; Laskar, 2020; Schwarzacher, 1993; Weedon, 2003), neither of which characterized the subtropical study area in Albian times.

The astronomical origin is supported by the EHA aimed at the lower-period cyclicity. This EHA revealed a characteristic pattern, which contains a main band (centred at a period of 0.7 m, the average thickness of the lithological alternation attributed to precession cycles) that splits into two period bands with different power at 2–3 m and 5.5–6.5 m of the studied succession (Fig. 6). Previous studies demonstrated that similar signal bifurcations in evolutionary spectra can result from the occurrence of hiatuses (Meyers et al., 2001). However, there is no evidence of hardgrounds in the studied section and the boundaries between successive beds are gradational, suggesting that sedimentation was continuous. Other studies showed that signal bifurcations in EHA spectra can also be produced at short-eccentricity and precession bandwidths due to frequency and amplitude modulation at long-eccentricity (405 ky) cycle minima (Dinarès-Turell et al., 2018; Intxauspe-Zubiaurre et al., 2018; Laurin et al., 2016; Li et al., 2019; Martínez-Braceras et al., 2022). However, in the studied succession the distance of 3.5 m between successive bifurcations of the precessional

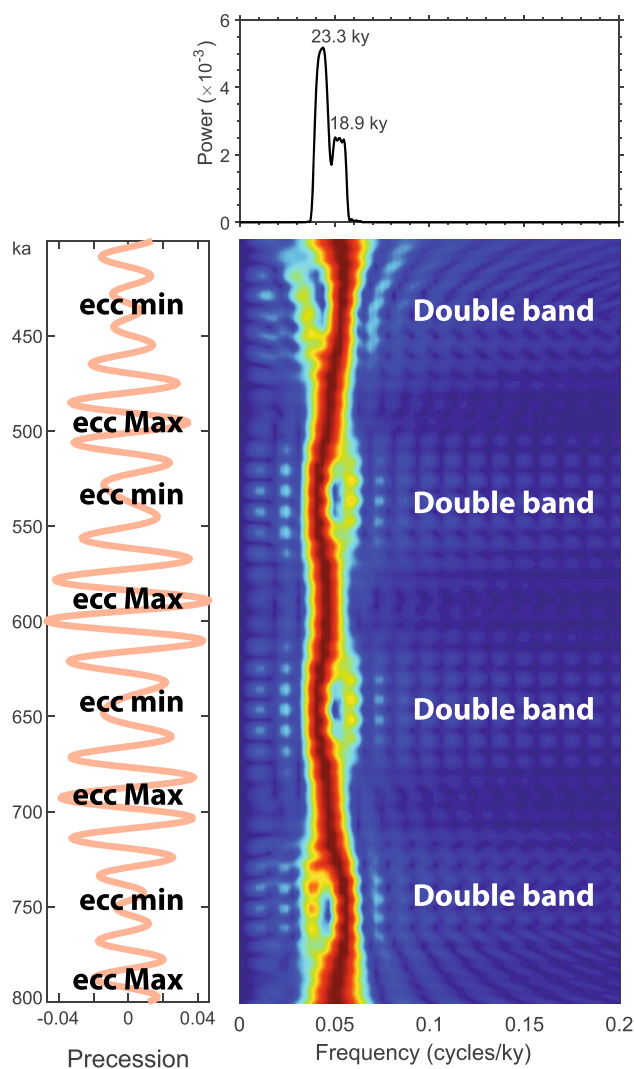
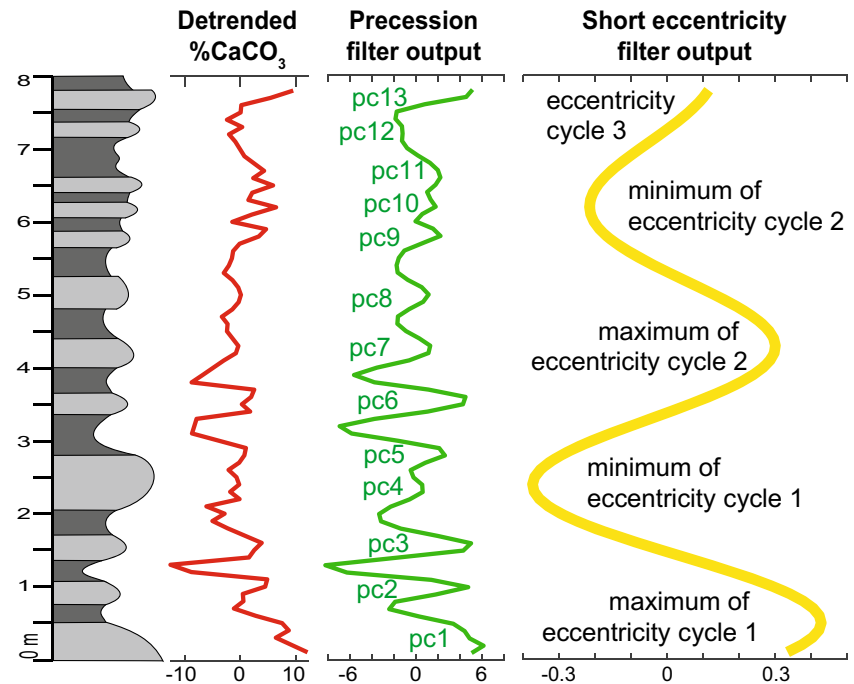


Fig. 7 Precession index for the 800–400-ka interval from the La04 orbital solution (Laskar et al., 2004). The 2π -MTM and evolutionary spectra show the amplitude and frequency modulation of precession cycles by short eccentricity cycles: a single precession frequency band characterizes short-eccentricity maxima (ecc Max), whereas double precession bands, one with higher power than the other, occur at short-eccentricity minima (ecc min)

band agrees with the period attributed to short-eccentricity cycles. To our knowledge, amplitude and frequency modulation of the precessional signal by short-eccentricity cycles has not been described before in evolutionary spectra. In order to test whether short-eccentricity cycles can really modulate the expression of precession cycles in evolutionary spectra, an EHA was performed using the standard precessional solution of the 400–800 ka interval, which shows a clear overprinting of short-eccentricity cycles (Laskar et al., 2004, 2011). The result shows a main precession band which forks into two bands, one with higher power and the other with lower power, when precession driven fluctuations display minimum amplitude,

Fig. 8 Lithological log of the studied succession, the detrended %CaCO₃ record (in red in the left-hand side graph), and Gaussian bandpass filter outputs. Filters targeted the main periods identified in the spectral analysis, which correspond to precession cycles (pc) (middle graph in green; Gaussian bandpass frequency 1.47 ± 1) and short eccentricity cycles (in yellow in the right-hand side graph; Gaussian bandpass frequency 0.28 ± 0.02)



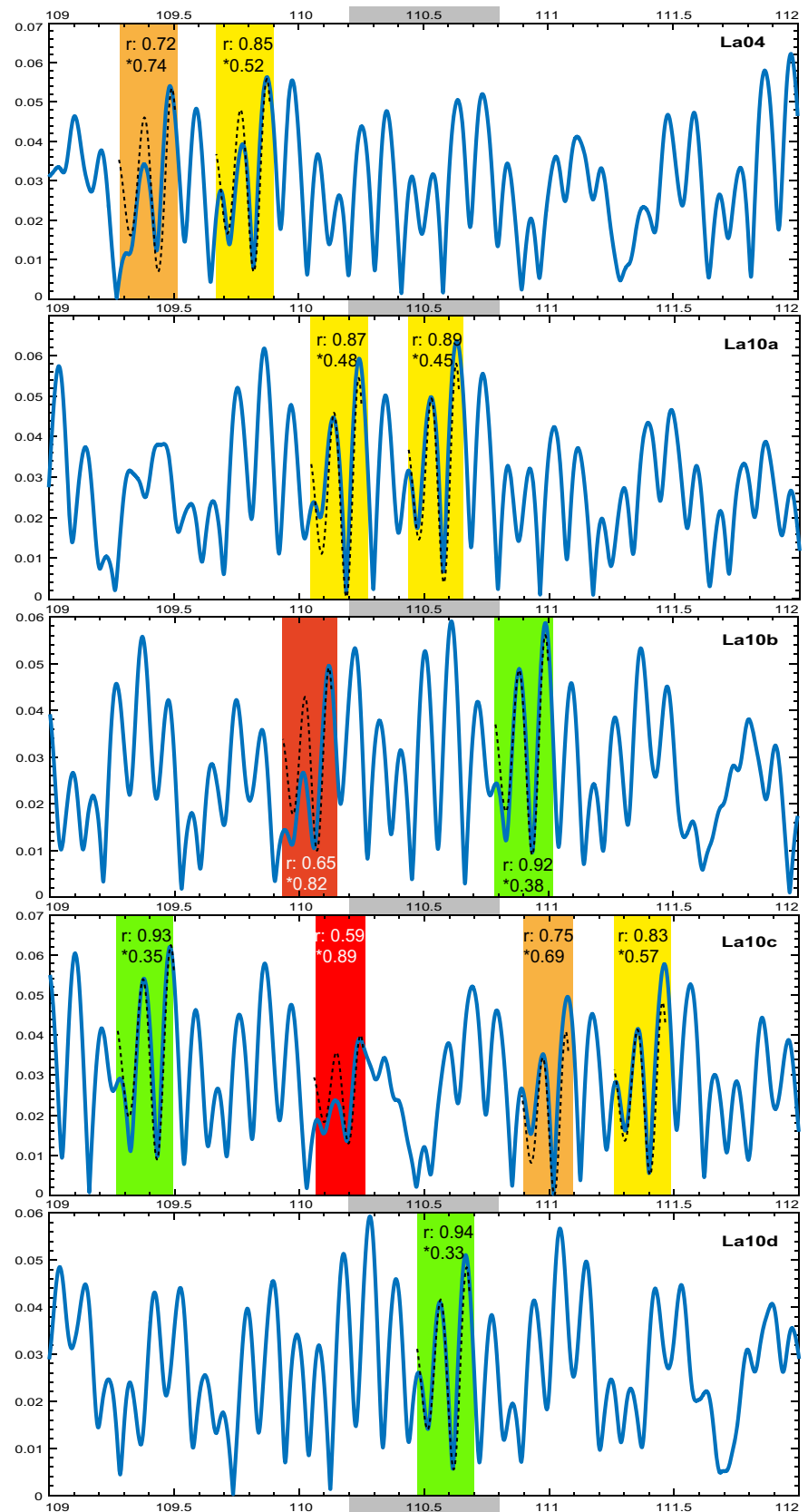
which occurs at short-eccentricity minima (Fig. 7). This demonstrates that the intervals with a single precessional band in evolutionary spectra correspond to short-eccentricity maxima, whereas bifurcations represent short-eccentricity minima. Accordingly, the bifurcations at 2–3 m and 5.5–6.5 m of the studied succession are attributed to short-eccentricity minima and allow definition of a complete short-eccentricity bundle in between (Fig. 6). Following on from this interpretation, the upper part of another short-eccentricity bundle must occur in the lower part of the succession, whereas the upper part of the succession must correspond to part of a third short-eccentricity cycle.

In order to better characterize the Milankovitch-band cyclicity of the studied succession, the precession and short-eccentricity components recorded in the %CaCO₃ data series were extracted separately by Gaussian bandpass filtering. To this end, the average frequency values of the two most significant bands identified in the spectral analysis were used, allowing sufficiently ample bandwidth (Fig. 8). The highest frequency bandpass filtering produced thirteen precession cycles that match precisely the couplets identified in the succession (taking into account the composite nature of bed 7, as revealed by its %CaCO₃ content), thus demonstrating the reliability of the filtering technique. Furthermore, the filtered precession signal shows amplitude modulation in line with the short-eccentricity cycles defined above, with low-amplitude precession cycles at eccentricity minima (pc 4–5 and pc9–11 in Fig. 8) and higher-amplitude precession cycles at eccentricity maxima. The lower-frequency filtering output shows three short-eccentricity

cycles (a first high-amplitude cycle followed by a second intermediate-amplitude cycle and a third low-amplitude cycle), although the oldest and youngest cycles are not fully recorded (Fig. 8).

Direct comparison of the Cotoño-Mioño %CaCO₃ filter outputs with orbital solutions is hindered due to several factors. Firstly, orbital forcing is not linearly transferred to climate change and to depositional processes, meaning that the depositional record is generally not a linear representation of the primary forcing. Secondly, even if linear comparison between depositional records and orbital solutions were possible, the short extent of the studied succession could prevent accurate correlation. Finally, the tuning of precession and short-eccentricity cycles to astronomical solutions is not reliable beyond 50–60 Ma (Hinnov, 2013; Laskar, 2020; Laskar et al., 2011; Zeebe & Lourens, 2019). This is due to theoretical uncertainties produced by the chaotic behaviour of large bodies within the asteroid belt, which preclude calculation of a unique orbital solution. Despite these hindrances, a tentative comparison between the short-eccentricity filter output of the studied data series and available astronomical solutions was carried out (Laskar et al., 2004, 2011). The target interval was 109–112 Ma, as the studied succession was formed during the early Albian Raulinianus and Puzosianus ammonite Subzones of the Auritiformis Zone and the Mammillatum Superzone, which according to Gale et al. (2020) corresponds to 110.2–110.8 Ma. A succession of short-eccentricity cycles with an arrangement similar to

Fig. 9 Comparison of the short-eccentricity (100 ky) filter output obtained from the Cotohino-Mioño data and available orbital solutions for the 112–109 Ma interval (Laskar et al., 2004, 2011). The Cotohino-Mioño filter output is characterized by a first high-amplitude cycle followed by a second intermediate-amplitude cycle and a third low-amplitude cycle (Fig. 8). A similar arrangement is observed at 11 intervals of the orbital solutions (target intervals highlighted with coloured bands). For visual comparison, the Cotohino-Mioño filter output is shown as a broken black line on each target interval. The Pearson correlation coefficient (r) and the root-mean-square deviation (RMSD, represented by an asterisk) of the amplitude modulation at each interval were calculated ($r > 0.90$ and $\text{RMSD} < 0.4$ at green bands; $r: 0.80\text{--}0.89$ and $\text{RMSD}: 0.41\text{--}0.6$ at yellow bands; $r: 0.70\text{--}0.79$ and $\text{RMSD}: 0.61\text{--}0.8$ at orange bands; $r < 0.69$ and $\text{RMSD} > 0.8$ at red bands), demonstrating that only three intervals in solutions La10b, La10c and La10d show potential correlation with the Cotohino-Mioño filter output. The grey band at the horizontal chronological scale bar (in Ma) shows the age of the studied deposits according to biostratigraphic data. Tentative tuning to the 110.68–110.47 Ma interval in La10d is the logical choice



that produced by the Cotolino-Mioño filtered signal (high, intermediate and low-amplitude cycles; Fig. 8) was found at 11 intervals of the analyzed orbital solutions, allowing various potential correlation frameworks (Fig. 9). In order to solve the uncertainty, the statistical significance of each correlation was determined by calculating the Pearson correlation coefficient (r) and the root-mean-square deviation (RMSD) between the Cotolino-Mioño filter output and the target intervals of the orbital solutions. Only correlation with three intervals of the orbital solutions (namely the 111–110.79 Ma interval in solution La10b, the 109.49–109.28 Ma interval in solution La10c, and

the 110.68–110.47 Ma interval in solution La10d) show r values higher than 0.9 and relatively low RMSD values, which suggest reliable correlation (Fig. 9; Online Resource 4). Taking into account the 110.8–110.2 Ma age derived from biostratigraphic data, tentative tuning to solution La10d is the logical choice, which in fact shows the highest correlation coefficient ($r > 0.94$) and lowest deviation (RMSD < 0.34).

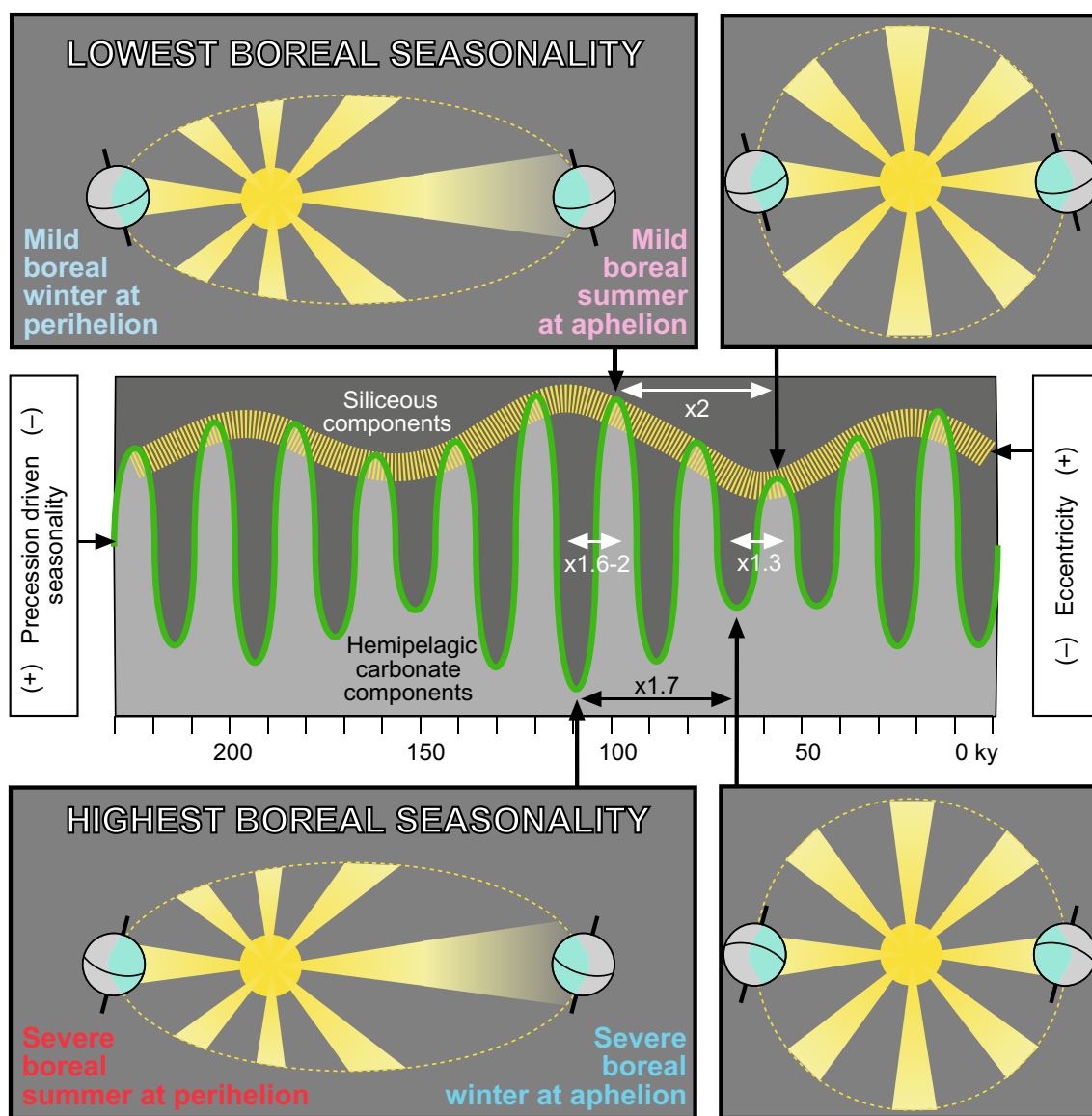


Fig. 10 Conceptual model showing the astronomical configurations leading to hemipelagic limestone accumulation (top) and marlstone sedimentation (bottom) in the Castro Urdiales area in Albian times, as a consequence of insolation and seasonality variations driven by

precession (ca. 20 ky) and short-eccentricity (ca. 100 ky) cycles (middle graph). The magnitude by which carbonate production and/or siliceous dilution varied at precessional and eccentricity timescales is also shown in the astronomical model in the middle

5.2 The nature of the cyclic environmental changes

Astronomically forced climate-change cycles can affect hemipelagic sedimentation through periodic fluctuations in three main environmental processes: carbonate dissolution, carbonate production and siliceous dilution (either by detrital clays or intrabasinal siliceous particles), all of which are linked to seasonality variations at precessional timescales (Einsele & Ricken, 1991; Einsele et al., 1991; Gambacorta et al., 2019; Martínez, 2018). Alternating hemipelagic limestones and marlstones can be created by syndimentary carbonate dissolution when periodic variations in seawater CO₂ content result in the depositional site alternately being above and below the carbonate compensation depth. This environmental process can be readily disregarded for the studied succession, as the 225–250 m deep area was well above the lysocline. Climatically driven fluctuations in carbonate production are the result of cyclic variations in the supply of fine-grained micrite derived from adjacent shallow-water areas and in the populations of planktonic foraminifera and calcareous nannoplankton. Hemipelagic alternations formed in response to such fluctuations in carbonate production are typically characterized by thick limestone beds and thin marlstone beds (Batenburg et al., 2014; Einsele & Ricken, 1991; Gambacorta et al., 2019; Martínez-Braceras et al., 2017). Finally, hemipelagic alternations can also result from periodic fluctuations in the rate of dilution of pelagic carbonate sediment with siliceous components, most commonly terrestrial clay and silt. In such cases, the hemipelagic successions generally show thick marlstone beds and thin limestone beds (Batenburg et al., 2014; Einsele & Ricken, 1991; Martínez-Braceras et al., 2017; Payros & Martínez-Braceras, 2014).

The assessment of the variations in carbonate production and siliceous dilution in the studied deposits was not straightforward, as the limestone/marlstone thickness ratio varies significantly along the succession (Fig. 4). However, it is reasonable to assume that carbonate sedimentation increased in the studied area when calcareous plankton thrived in pelagic seawaters and/or the rate of carbonate mud production on shallow-water areas exceeded the accommodation rate, surpluses being exported basinwards. Both processes require stable seawater conditions over long periods, with sustained high temperatures throughout the year, reduced vertical mixing, and increased stratification leading to warm and oligotrophic surficial waters (Beaufort et al., 2022; Bellanca et al., 1996; Hopkins et al., 2015; Poletti et al., 2004). At precessional timescales, such stable seawater conditions are favoured when annual seasonality is reduced (Fig. 10), which in the northern hemisphere happens when winter occurs at perihelion (i.e., when the Earth is closest to the Sun) and when summer occurs at aphelion (furthest from the Sun).

Conversely, it can be assumed that hemipelagic marlstones accumulated in the area when carbonate production decreased and/or when siliceous dilution increased (Fig. 10). Siliceous dilution could have been caused by either terrestrially derived siliciclastic sediment supply or siliceous particle production by sponges. The rate of terrestrial siliciclastic input is closely related to climate, reaching maximum values under increased seasonality with just three to five wet months per year (Cecil & Dulong, 2003). Regarding siliceous sponges, on the basis of extant analogues Rosales et al. (1995) concluded that long-term mass occurrences in the studied area were related to the intensification of basinward-directed bottom currents rich in organic matter (also see Astibia et al., 2014; Maldonado et al., 2005). Both terrestrial siliciclastic input and intensified seawater circulation are favoured by significant seasonal contrast throughout the year. Taking everything into account, it can be concluded that marlstones accumulated in the studied area when annual seasonality increased, which at precessional timescales happens when boreal summer occurs at perihelion and winter at aphelion (Fig. 10).

The %CaCO₃ record can further be used to assess the magnitude by which the abovementioned environmental factors varied due to astronomically forced climate change at precessional and short-eccentricity timescales (De Boer, 1991; Einsele & Ricken, 1991; Martínez-Braceras et al., 2017; Payros & Martínez-Braceras, 2014; Ricken, 1991). At precessional timescales, the difference in carbonate content in successive limestone and marlstone beds varied between 11 and 17% (average 14%) at maximum eccentricity. If carbonate production remained constant throughout a precession cycle at maximum eccentricity, such variations would imply that siliceous dilution varied by an average factor of 1.6 during opposite precessional configurations. However, if siliceous dilution remained constant at maximum eccentricity, the %CaCO₃ variations recorded in a precession cycle would imply that carbonate production increased and decreased twofold (Fig. 10). At minimum eccentricity the difference in carbonate content in successive limestone and marlstone beds was attenuated, diminishing to 1–8% (average 5%). This means that, regardless of the main environmental process affected by seasonality variations at precessional timescales, either carbonate productivity or siliceous dilution changed by a factor of approximately 1.3 (Fig. 10).

Beds with similar lithology (i.e., formed at the same precessional configuration) can also be compared at minimum and maximum eccentricity. The difference of up to 13% in carbonate content found in limestone beds suggests that either carbonate productivity or siliceous dilution varied twofold due to varying eccentricity when precession driven seasonality was low (Fig. 10). The

%CaCO₃ differences between marlstone beds formed at maximum and minimum eccentricity were slightly lower (less than 10%), meaning that the influence of the controlling environmental factor varied by less than a factor of 1.7 due to eccentricity variations when precession driven seasonality was high (Fig. 10). Given that eccentricity driven variations in insolation are known to be very small (ca. 0.2%; Weedon, 2003), it is reasonable to conclude that the variations in the rate of carbonate production and/or siliceous dilution caused by precession driven climate change must have been amplified by some positive feedback mechanisms. This shows that some environmental processes are highly sensitive to minor variations in climatic parameters.

6 Conclusions

Some of the characteristics found in the Albian Mioño Formation of the Castro Urdiales area show evidence of diagenetic overprinting, including partial recrystallization, occurrence of dispersed pyrite and fluid-escape structures, and magnetic susceptibility values unrelated to lithology. However, the sedimentological, petrographic and cyclostratigraphic analysis carried out herein demonstrates that the hemipelagic carbonate alternation was originally astronomically forced. Thirteen precession couplets, arranged in one complete plus two partial short-eccentricity bundles, were identified through several spectral analysis techniques and Gaussian bandpass filtering. Biostratigraphic age data (Rosales, 1995, calibrated to Gale et al., 2020) and tentative tuning to orbital solution La10d (Laskar et al., 2011) suggest that the studied succession accumulated 110.68–110.47 Ma in an outer ramp setting at 225–250 m water depth. Annual seasonality fluctuations driven by precession cycles caused periodic (20 ky) variations in the rate of carbonate productivity and/or siliceous dilution. These variations resulted in the formation of marly limestone beds when annual seasonality was low (i.e., boreal summer at aphelion, winter at perihelion) and the accumulation of marlstones when seasonality increased (i.e., boreal summer at perihelion, winter at aphelion). The incidence of these processes increased and decreased in line with seasonality modulation by short-eccentricity cycles of 100 ky.

The studied hemipelagic deposits formed during the rifting phase of the Basque-Cantabrian Basin, which was characterized by synsedimentary faulting, block tilting, volcanism and hydrothermal activity related to strong extensional and/or transtensional tectonics. Tectonically driven instabilities are generally thought to suppress the effects of more subtle environmental processes, such as climate change, imprinting the sedimentary record accordingly. However, this case study shows that

Milankovitch cycles can be reliably identified in hemipelagic successions accumulated in tectonically active sedimentary settings if sediment gravity flows or other disturbances do not affect autochthonous sedimentation.

Supplementary Information The online version contains supplementary material available at <https://doi.org/10.1007/s41513-022-00198-z>.

Acknowledgements Research funded by the MCIN/AEI project PID2019-105670GB-I00/AEI/10.13039/501100011033 of the Spanish Government and by the Consolidated Research Group IT1602-22 of the Basque Government. NM-B is grateful for post-doctoral specialization grants DOCREC19/35 and ESPDOC21/49 of the University of the Basque Country (UPV/EHU). Thanks are due to Nestor Vegas (UPV/EHU) for assistance with magnetic susceptibility measurements and to Carl Sheaver for his language corrections. Comments by journal editor J.C. Braga and two reviewers (B. Bádenas and anonymous) helped to improve the original manuscript.

Author contributions AP conceived the study, participated in the fieldwork, carried out the petrographic, magnetic susceptibility, calcimeter and spectral analyses, interpreted the results and wrote the manuscript. NM-B participated in the fieldwork, carried out the magnetic susceptibility and spectral analyses, and contributed to interpreting the results and writing the manuscript. LMA participated in the fieldwork, carried out the petrographic and magnetic susceptibility analyses, and contributed to interpreting the results and writing the manuscript. JD-T carried out spectral analysis and contributed to interpreting the results and writing the manuscript. IR provided crucial geological and biostratigraphic information and contributed to writing the manuscript. All co-authors read and approved the final version of the manuscript, and gave consent for submission for possible publication to the JOURNAL OF IBERIAN GEOLOGY. AP: Conceptualization, methodology, software, validation, formal analysis, investigation, writing—original draft, writing—review and editing, visualization, supervision, project administration, funding acquisition. NM-B: software, formal analysis, investigation, writing—review and editing. LMA: investigation, writing—review and editing. JD-T: software, investigation, writing—review and editing. IR: investigation, writing—review and editing.

Funding Open Access funding provided thanks to the CRUE-CSIC agreement with Springer Nature. Research funded by the MCIN/AEI project PID2019-105670GB-I00/AEI/10.13039/501100011033 of the Spanish Government and by the Consolidated Research Group IT1602-22 of the Basque Government.

Availability of data and material Quantitative raw data used to carry out the analysis and generate figures is available online at the journal's website as Supplementary Information (Online Resources 1–4).

Code availability The Acycle software used to carry out the spectral analysis is available at <https://acycle.org/>. This software includes the orbital solutions referred to in our study.

Declarations

Conflict of interest The authors declare neither conflicts of interests nor competing interests. This is an original work based on the authors' scientific data and interpretations. Authorship credit is duly given to previous work when necessary. The manuscript has been specifically

prepared with the JOURNAL OF IBERIAN GEOLOGY in mind, and has not been submitted for publication elsewhere.

Open Access This article is licensed under a Creative Commons Attribution 4.0 International License, which permits use, sharing, adaptation, distribution and reproduction in any medium or format, as long as you give appropriate credit to the original author(s) and the source, provide a link to the Creative Commons licence, and indicate if changes were made. The images or other third party material in this article are included in the article's Creative Commons licence, unless indicated otherwise in a credit line to the material. If material is not included in the article's Creative Commons licence and your intended use is not permitted by statutory regulation or exceeds the permitted use, you will need to obtain permission directly from the copyright holder. To view a copy of this licence, visit <http://creativecommons.org/licenses/by/4.0/>.

References

- Agirrezabala, L. M. (2015). Syndepositional forced folding and related fluid plumbing above a magmatic laccolith: Insights from outcrop (Lower Cretaceous, Basque-Cantabrian Basin, western Pyrenees). *Geological Society of America Bulletin*, 127, 982–1000.
- Agirrezabala, L. M., & García-Mondéjar, J. (1992). Tectonic origin of carbonate depositional sequences in a strike-slip setting (Aptian, northern Iberia). *Sedimentary Geology*, 81, 163–172.
- Astibia, H., Elorza, J., Pisera, A., Alvarez-Perez, G., Payros, A., & Ortiz, S. (2014). Sponges and corals from the middle Eocene (Bartonian) marly formations of the Pamplona Basin (Navarre, western Pyrenees): Taphonomy, taxonomy and paleoenvironments. *Facies*, 60, 91–110.
- Batenburg, S. J., Gale, A. S., Sprovieri, M., Hilgen, F. J., Thibault, N., Boussaha, M., & Orue-Etxebarria, X. (2014). An astronomical time scale for the Maastrichtian based on the Zumaia and Sopelana sections (Basque country, northern Spain). *Journal of the Geological Society*, 171, 165–180.
- Batenburg, S. J., Sprovieri, M., Gale, A. S., Hilgen, F. J., Hüsing, S., Laskar, J., Liebrand, D., Lirer, F., Orue-Etxebarria, X., Pelosi, N., & Smit, J. (2012). Cyclostratigraphy and astronomical tuning of the Late Maastrichtian at Zumaia (Basque country, Northern Spain). *Earth and Planetary Science Letters*, 359, 264–278.
- Beaufort, L., Bolton, C. T., Sarr, A. C., Suchéras-Marx, B., Rosenthal, Y., Donnadieu, Y., Barbarin, N., Bova, S., Cornault, P., Gally, Y., Gray, E., Mazur, J. C., & Tetard, M. (2022). Cyclic evolution of phytoplankton forced by changes in tropical seasonality. *Nature*, 601, 79–84.
- Bellanca, A., Claps, M., Erba, E., Masetti, D., Neri, R., Premoli Silva, I., & Venezia, F. (1996). Orbitally induced limestone/marlstone rhythms in the Albian-Cenomanian Cison section (Venetian region, northern Italy): Sedimentology, calcareous and siliceous plankton distribution, elemental and isotope geochemistry. *Palaeogeography Palaeoclimatology Palaeoecology*, 126, 227–260.
- Bodego, A., & Agirrezabala, L. M. (2013). Syn-depositional thin- and thick-skinned extensional tectonics in the mid-Cretaceous Lasarte sub-basin, western Pyrenees. *Basin Research*, 25, 594–612.
- Boulila, S., De Rafelis, M., Hinnov, L. A., Gardin, S., Galbrun, B., & Collin, P. (2010). Orbitally forced climate and sea-level changes in the Paleocene Tethyan domain (marl-limestone alternations, Lower Kimmeridgian, SE France). *Palaeogeography Palaeoclimatology Palaeoecology*, 292, 57–70.
- Cantalejo, B., & Pickering, K. T. (2015). Orbital forcing as principal driver for fine-grained deep-marine siliciclastic sedimentation, Middle Eocene Ainsa Basin, Spanish Pyrenees. *Palaeogeography Palaeoclimatology Palaeoecology*, 421, 24–47.
- Cecil, C. B., & Dulong, F. T. (2003). Precipitation models for sediment supply in warm climates. In C. B. Cecil & N. T. Edgar (Eds.), *Climate controls on stratigraphy. SEPM Special Publications* (Vol. 77, pp. 21–27). Society for Sedimentary Geology.
- De Benedictis, D., Bosence, D., Waltham, D. (2007). Tectonic control on peritidal carbonate parasequence formation: an investigation using forward tectono-stratigraphic modelling. *Sedimentology*, 54, 587–605.
- De Boer, P. L. (1991). Pelagic black shale-carbonate rhythms: Orbital forcing and oceanographic response. In G. Einsele, W. Ricken, & A. Seilacher (Eds.), *Cycles and events in stratigraphy* (pp. 63–78). Springer.
- De Boer, P. L., & Smith, D. G. (1994). Orbital forcing and cyclic sequences. In P. L. De Boer & D. G. Smith (Eds.), *Orbital forcing and cyclic sequences. IAS Special Publication* (Vol. 19, pp. 1–14). International Association of Sedimentologists.
- Dinarès-Turell, J., Baceta, J. I., Pujalte, V., Orue-Etxebarria, X., Bernaola, G., & Lorito, S. (2003). Untangling the Palaeocene climatic rhythm: An astronomically calibrated early Palaeocene magnetostratigraphy and biostratigraphy at Zumaia (Basque basin, northern Spain). *Earth and Planetary Science Letters*, 216, 483–500.
- Dinarès-Turell, J., Martínez-Bracerás, N., & Payros, A. (2018). High-resolution integrated cyclostratigraphy from the Oyambre section (Cantabria, N Iberian peninsula): Constraints for orbital tuning and correlation of middle Eocene Atlantic deep-sea records. *Geochemistry Geophysics Geosystems*, 19, 787–806.
- Dinarès-Turell, J., Westerhold, T., Pujalte, V., Röhl, U., & Kroon, D. (2014). Astronomical calibration of the Danian stage (Early Paleocene) revisited: Settling chronologies of sedimentary records across the Atlantic and Pacific Oceans. *Earth and Planetary Science Letters*, 405, 119–131.
- Einsele, G., & Ricken, W. (1991). Limestone-marl alternation: An overview. In G. Einsele, W. Ricken, & A. Seilacher (Eds.), *Cycles and events in stratigraphy* (pp. 23–47). Springer.
- Einsele, G., Ricken, W., & Seilacher, A. (1991). *Cycles and events in stratigraphy*. Springer.
- Elderbak, K., & Leckie, R. M. (2016). Paleocirculation and foraminiferal assemblages of the Cenomanian-Turonian Bridge Creel Limestone bedding copulets: Productivity vs. dilution during OAE2. *Cretaceous Research*, 60, 52–77.
- Fenner, J. (2001). Palaeoceanographic and climatic changes during the Albian, summary of the results from the Kirchrode boreholes. *Palaeogeography Palaeoclimatology Palaeoecology*, 174, 287–304.
- Ferguson, I. J., Da Silva, A. C., Chow, N., & George, A. D. (2021). Interplay of eutatic, tectonic and autogenic controls on a Late Devonian carbonate platform, northern Canning Basin, Australia. *Basin Research*, 33, 312–341.
- Fernandez-Mendiola, P. A., & Garcia-Mondejar, J. (1995). Carbonate platform growth influenced by contemporaneous basaltic intrusion (Albian of Larrano, Spain). *Sedimentology*, 50, 961–978.
- Gale, A. S., Mutterlose, J., & Batenburg, S. (2020). The Cretaceous Period. In F. M. Gradstein, J. G. Ogg, M. D. Schmitz, & G. M. Ogg (Eds.), *Geologic Times Scale 2020* (pp. 1023–1086). Elsevier.
- Gambacorta, G., Malinverno, A., & Erba, E. (2019). Orbital forcing of carbonate versus siliceous productivity in the late Albian-late Cenomanian (Umbria-Marche Basin, central Italy). *Newsletters on Stratigraphy*, 52, 197–220.

- García-Mondéjar, J. (1990). The Aptian-Albian carbonate episode of the Basque-Cantabrian basin, northern Spain: general characteristics, controls and evolution. In M. E. Tucker, J. L. Wilson, P. D. Crevello, J. R. Sarg, & J. F. Read (Eds.), *Carbonate platforms, facies and sequences. IAS Special Publication* (Vol. 9, pp. 257–290). International Association of Sedimentologists.
- García-Mondéjar, J., Agirrezabal, L. M., Aranburu, A., Fernandez-Mendiola, P. A., Gomez-Perez, I., Lopez-Horgue, M., & Rosales, I. (1996). Aptian-Albian tectonic pattern of the Basque-Cantabrian Basin (northern Spain). *Geological Journal*, *31*, 13–45.
- Hallam, A. (1986). Origin of minor limestone-shale cycles – climatically induced or diagenetic. *Geology*, *14*, 609–612.
- Hay, W. W., DeConto, R., Wold, C. N., Wilson, K. M., Voigt, S., Schulz, M., Wold-Rossby, A., Dullo, W. C., Ronov, A. B., Balukhovskiy, A. N., & Soeding, E. (1999). Alternative global Cretaceous paleogeography. In E. Barrera & C. Johnson (Eds.), *The evolution of Cretaceous ocean/climate systems. GSA Special Paper* (Vol. 332, pp. 1–47). Geological Society of America.
- Hinnov, L. A. (2013). Cyclostratigraphy and its revolutionizing applications in the earth and planetary sciences. *Geological Society of America Bulletin*, *125*, 1703–1734.
- Hopkins, J., Henson, S. A., Painter, S. C., Tyrrell, T., & Poulton, A. J. (2015). Phenological characteristics of global coccolithophore blooms. *Global Biogeochemical Cycles*, *29*, 239–253.
- Intxauspe-Zubiaurre, B., Martínez-Braceras, N., Payros, A., Ortiz, S., Dinarès-Turell, J., & Flores, J. A. (2018). The last Eocene hyperthermal (Chron C19r event, ~41.5 Ma): Chronological and paleoenvironmental insights from a continental margin (Cape Oyambre, N Spain). *Palaeogeography Palaeoclimatology Palaeoecology*, *505*, 198–216.
- Jimenez-Berrocoso, A., Elorza, J., & MacLeod, K. G. (2013). Proximate environmental forcing in fine-scale geochemical records of calcareous couplets (Upper Cretaceous and Palaeocene of the Basque-Cantabrian Basin, eastern North Atlantic). *Sedimentary Geology*, *284*, 76–90.
- Jones, M. M., Sagerman, B. B., Oakes, R. L., Parker, A. L., Leckie, R. M., Bralower, T. J., Sepulveda, J., & Fortiz, V. (2019). Astronomical pacing of relative sea level during Oceanic Anoxic Event 2: Preliminary studies of the expanded SH#1 core, Utah, USA. *Geological Society of America Bulletin*, *131*, 1702–1722.
- Kodama, K. P., Anastasio, D. J., Newton, M. L., Pares, J. M., & Hinnov, L. A. (2010). High-resolution rock magnetic cyclostratigraphy in an Eocene flysch, Spanish Pyrenees. *Geochemistry Geophysics Geosystems*, *11*, Q0AA07.
- Kodama, K. P., & Hinnov, L. A. (2015). *Rock magnetic cyclostratigraphy*. Wiley.
- Laskar, J. (2020). Astrochronology. In F. M. Gradstein, J. G. Ogg, M. D. Schmitz, & G. M. Ogg (Eds.), *Geologic times scale 2020* (pp. 139–158). Elsevier.
- Laskar, J., Fienga, A., Gastineau, M., & Manche, H. (2011). La2010: A new orbital solution for the long-term motion of the Earth. *Astronomy & Astrophysics*, *532*, A89.
- Laskar, J., Robutel, P., Joutel, F., Gastineau, M., Correia, A. C. M., & Levrard, B. (2004). A long-term numerical solution for the insolation quantities of the Earth. *Astronomy & Astrophysics*, *428*, 261–285.
- Laurin, J., Meyers, S. R., Galeotti, S., & Lanci, L. (2016). Frequency modulation reveals the phasing of orbital eccentricity during Cretaceous Oceanic Anoxic Event II and the Eocene hyperthermals. *Earth and Planetary Science Letters*, *442*, 143–156.
- Laurin, J., & Sagerman, B. B. (2007). Cenomanian-Turonian coastal record in SW Utah, U.S.A.: Orbital-scale transgressive-regressive events during Oceanic Anoxic Event II. *Journal of Sedimentary Research*, *77*, 731–756.
- Li, M. S., Hinnov, L., & Kump, L. (2019). Acycle: Time-series analysis software for paleoclimate research and education. *Computers & Geosciences*, *127*, 12–22.
- Lopez-Horgue, M. A., Iriarte, E., Schröder, S., Fernandez-Mendiola, P. A., Caline, B., Corneillie, H., Frémont, J., Sudrie, M., & Zerti, S. (2010). Structurally controlled hydrothermal dolomites in Albian carbonates of the Ason valley, Basque-Cantabrian Basin, northern Spain. *Marine and Petroleum Geology*, *27*, 1069–1092.
- Maldonado, M., Carmona, M. C., Velasquez, Z., Puig, A., Cruzado, A., Lopez, A., & Young, C. M. (2005). Siliceous sponges as a silicon sink: An overlooked aspect of benthopelagic coupling in the marine silicon cycle. *Limnology and Oceanography*, *50*, 799–809.
- Mann, M. E., & Lees, J. M. (1996). Robust estimation of background noise and signal detection in climatic time series. *Climatic Change*, *33*, 409–445.
- Marshall, J. D. (1992). Climatic and oceanographic isotopic signals from the carbonate rock record and their preservation. *Geological Magazine*, *129*, 143–160.
- Martinez, M. (2018). Chapter four—Mechanisms of preservation of the eccentricity and longer-term Milankovitch cycles in detrital supply and carbonate production in hemipelagic marl-limestone alternations. In M. Monenari (Ed.), *Cyclostratigraphy and astrochronology* (pp. 189–218). Elsevier.
- Martínez-Braceras, N., Franceschetti, G., Payros, A., Monechi, S., & Dinarès-Turell, J. (2022). High-resolution cyclochronology of the lowermost Ypresian Arnakatxa section (Basque-Cantabrian Basin, western Pyrenees). *Newsletters on Stratigraphy*. <https://doi.org/10.1127/nos/2022/0706>
- Martínez-Braceras, N., Payros, A., Miniati, F., Arostegi, J., & Franceschetti, G. (2017). Contrasting environmental effects of astronomically driven climate change on three Eocene hemipelagic successions from the Basque-Cantabrian Basin. *Sedimentology*, *64*, 960–986.
- Meyers, S. R. (2012). Seeing red in cyclic stratigraphy: Spectral noise estimation for astrochronology. *Paleoceanography*, *27*, PA3228.
- Meyers, S. R., Sagerman, B. B., & Hinnov, L. A. (2001). Integrated quantitative stratigraphy of the Cenomanian-Turonian Bridge Creek Limestone Member using evolutive harmonic analysis and stratigraphic modeling. *Journal of Sedimentary Research*, *71*, 628–644.
- Miró, J., Manatschal, G., Cadenas, P., & Muñoz, J. A. (2021). Reactivation of a hyperextended rift system: The Basque-Cantabrian Pyrenees case. *Basin Research*, *33*, 3077–3101.
- Mount, J., & Ward, P. (1986). Origin of limestone/marl alternations in the Upper Maastrichtian of Zumaya, Spain. *Journal of Sedimentary Petrology*, *56*, 228–236.
- Owen, H. G. (1988). The ammonite zonal sequence and ammonite taxonomy in the Douvilleiceras mammillatum superzone (lower Albian) in Europe. *Bulletin of the British Museum (natural History) Geology Series*, *44*, 177–231.
- Payros, A., & Martínez-Braceras, N. (2014). Orbital forcing in turbidite accumulation during the Eocene greenhouse interval. *Sedimentology*, *61*, 1411–1432.
- Poletti, L., Silva, I. P., Masetti, D., Pipan, M., & Claps, M. (2004). Orbitally driven fertility cycles in the Palaeocene pelagic sequences of the Southern Alps (Northern Italy). *Sedimentary Geology*, *164*, 35–54.
- Preto, N., Spötl, C., Mietto, P., Gianolla, P., Riva, A., & Manfrin, S. (2005). Aragonite dissolution, sedimentation rates and carbon isotopes in deep-water hemipelagites (Livinallongo Formation, Middle Triassic, northern Italy). *Sedimentary Geology*, *181*, 173–194.
- Reuning, L., Reijmer, J. J. G., Betzler, C., Swart, P., & Bauch, T. (2005). The use of paleoceanographic proxies in carbonate periplatform settings: Opportunities and pitfalls. *Sedimentary Geology*, *175*, 131–152.

- Reuning, L., Reijmer, J. J. G., & Mattioli, E. (2006). Aragonite cycles: Diagenesis caught in the act. *Sedimentology*, *53*, 849–866.
- Ricken, W. (1991). Variations of sedimentation rates in rhythmically bedded sediments: Distinction between depositional types. In G. Einsele, W. Ricken, & A. Seilacher (Eds.), *Cycles and events in stratigraphy* (pp. 167–187). Springer.
- Rosales, I. (1995). *La plataforma carbonatada de Castro Urdiales (Aptiense/Albiense, Cantabria)*. PhD thesis, University of the Basque Country.
- Rosales, I. (1999). Controls on carbonate-platform evolution on active fault blocks: The Lower Cretaceous Castro Urdiales platform (Aptian-Albian, northern Spain). *Journal of Sedimentary Research*, *69*, 447–465.
- Rosales, I., Fernandez-Mendiola, P. A., & Garcia-Mondejar, J. (1994). Carbonate depositional sequence development on active fault blocks: The Albian in the Castro Urdiales area, northern Spain. *Sedimentology*, *41*, 861–882.
- Rosales, I., Mehl, D., Fernandez-Mendiola, P. A., & Garcia-Mondejar, J. (1995). An unusual poriferan community in the Albian of Islares (north Spain): Palaeoenvironmental and tectonic implications. *Palaeogeography Palaeoclimatology Palaeoecology*, *119*, 47–61.
- Schmitz, B., Pujalte, V., & Nuñez-Betelu, K. (2001). Climate and sea-level perturbations during the initial Eocene thermal maximum: Evidence from siliciclastic units in the Basque Basin (Ermua, Zumaia and Trabakua pass), northern Spain. *Palaeogeography Palaeoclimatology Palaeoecology*, *165*, 299–320.
- Schwarzacher, W. (1993). *Cyclostratigraphy and the Milankovitch theory*. Elsevier.
- Tavani, S., & Muñoz, J. A. (2012). Mesozoic rifting in the Basque-Cantabrian Basin (Spain): Inherited faults, transversal structures and stress perturbation. *Terra Nova*, *24*, 70–76.
- Thomson, D. J. (1982). Spectrum estimation and harmonic analysis. *Proceedings of the IEEE*, *70*, 1055–1096.
- Weedon, G. P. (2003). *Time-series analysis and cyclostratigraphy: Examining stratigraphic records of environmental cycles*. Cambridge University Press.
- Westphal, H., Bohm, F., & Bornholdt, S. (2004). Orbital frequencies in the carbonate sedimentary record: Distorted by diagenesis? *Facies*, *50*, 3–11.
- Westphal, H., Hilgen, F., & Munnecke, A. (2010). An assessment of the suitability of individual rhythmic carbonate successions for astrochronological application. *Earth Science Reviews*, *90*, 19–30.
- Zeebe, E., & Lourens, L. J. (2019). Solar system chaos and the Paleocene-Eocene boundary age constrained by geology and astronomy. *Science*, *365*, 926–929.